Deng *et al. Microstructures* 2023;3:2023044
DOI: 10.20517/microstructures.2023.42

Microstructures

Review

Open Access

Check for updates

Magnetic structures and correlated physical properties in antiperovskites

Sihao Deng[1,2], Hongde Wang[1,5], Lunhua He[1,3,4], Cong Wang[5]

[1]Spallation Neutron Source Science Center, Dongguan 523803, Guangdong, China.
[2]Institute of High Energy Physics, Chinese Academy of Sciences, Beijing 100049, China.
[3]Institute of Physics, Chinese Academy of Sciences, Beijing 100190, China.
[4]Songshan Lake Materials Laboratory, Dongguan 523808, Guangdong, China.
[5]School of Integrated Circuit Science and Engineering, Beihang University, Beijing 100191, China.

Correspondence to: Prof. Lunhua He, Institute of Physics, Chinese Academy of Sciences, Beijing 100190, China, E-mail: lhhe@ihep.ac.cn; Prof. Cong Wang, School of Integrated Circuit Science and Engineering, Beihang University, Beijing 100191, China. E-mail: congwang@buaa.edu.cn

How to cite this article: Deng S, Wang H, He L, Wang C. Magnetic structures and correlated physical properties in antiperovskites. *Microstructures* 2023;3:2023044. https://dx.doi.org/10.20517/microstructures.2023.42

Received: 21 Aug 2023 **First Decision:** 5 Sep 2023 **Revised:** 11 Sep 2023 **Accepted:** 21 Sep 2023 **Published:** 10 Nov 2023

Academic Editor: Danmin Liu **Copy Editor:** Fangyuan Liu **Production Editor:** Fangyuan Liu

Abstract

Compounds with perovskite structures have become one of the focuses in both materials science and condensed matter physics because of their fascinating physical properties and potential functionalities correlated to magnetic structures. However, the understanding of the intriguing physical properties is still at an exploratory stage. Herein, owing to the magnetic frustration prompted by Mn_6N or Mn_6C octahedra, the abounding magnetic structures of antiperovskites, including collinear antiferromagnetic, collinear ferromagnetic, collinear ferrimagnetic, non-collinear magnetic, and non-coplanar magnetic spin configurations, are systematically introduced through the updated coverage. In addition, owing to the "spin-lattice-charge" coupling of antiperovskites, a large number of physical properties, such as anomalous thermal expansion, giant magnetoresistance, anomalous Hall effect, piezomagnetic/baromagnetic effects, magnetocaloric effect, barocaloric effect, *etc.*, are summarized by combining the discussions of the determined magnetic structures. This review aims to clarify the current research progress in this field, focusing on the relationship between the magnetic structures and the correlated physical properties, and provides the conclusion and outlook on further performance optimization and mechanism exploration in antiperovskites.

Keywords: Antiperovskite, magnetic structures, physical properties, strong correlation material

INTRODUCTION

Since the 1980s, compounds with perovskite structures have become one of the focuses in both materials science and condensed matter physics because of their fascinating physical properties and potential functionalities. These properties include superconductivity, multiferroics, colossal magnetoresistance, negative thermal expansion (NTE), *etc.*[1-4]. In the antiperovskite compounds (antiperovskites) similar to the perovskite structure, numerous interesting physical properties have also been observed, such as NTE[5-25], giant magnetoresistance[26-27], anomalous Hall effect[28-30], piezomagnetic/baromagnetic effects[23,31-35], magnetocaloric effect[36-39], barocaloric effect[40,41], nearly zero temperature coefficient of resistivity[42-46], superconductivity[47,48], *etc*. Therefore, antiperovskites have gained significant attention. Nevertheless, the understanding of these abnormal physical properties is still in the exploratory stage, and the accumulation of experimental data and further deepening of theoretical research are required.

The so-called antiperovskite structure refers to a structure that is similar to perovskite. As shown in Figure 1, the face-centered position occupied by non-metallic elements, such as oxygen, in the original perovskite structure is occupied by transition group element atoms M, especially the magnetic element M = Mn, Fe, Ni, *etc*. The body center position originally occupied by metal elements is occupied by non-metallic elements N or C, and the original vertex position is occupied by metal element X, thus forming a lattice belonging to a cubic unit cell with chemical formula $M_3XN(C)$ (M = Mn, Fe, Ni; X = Zn, Ga, Cu, Al, In, Sn). Among them, face-centered magnetic atoms (such as Mn) and body-centered N (C) atoms can form NMn_6 or CMn_6 octahedra, and six magnetic atoms Mn are located at the six corners of the octahedron, which is prone to magnetic frustration. Thereby it generates the abounding magnetic structures, including collinear antiferromagnetic (AFM), collinear ferromagnetic (FM), collinear ferrimagnetic (FIM), non-collinear magnetic, and non-coplanar magnetic spin configurations[49-51]. On the other hand, the abundant magnetic structures in antiperovskite $Mn_3XN(C)$ compounds are very sensitive to changes in temperature, magnetic field, pressure, composition, and grain size. Its abnormal lattice change, magnetic phase transition, and electronic transport properties are interrelated and affect each other, showing its rich physical properties.

In this paper, we will summarize the magnetic structures and correlated physical properties in antiperovskites. We present the potential application of antiperovskites as novel materials in various emerging fields. In order to further optimize performance and explore mechanisms, the issues such as exploration of new magnetic structures, synthesis of single crystal samples, and practical application research for the in-depth research are deserved in the part of outlook.

MAGNETIC STRUCTURES IN MN-BASED ANTIPEROVSKITES

The research on the magnetic structures of antiperovskites mainly focuses on Mn-based compounds. Herein, the collinear, non-collinear, and non-coplanar magnetic structures in Mn-based antiperovskites will be introduced in this review.

Collinear magnetic structure

Both collinear AFM and collinear FM structures were determined by neutron diffraction in Mn_3GaC as early as the 1970s. Upon warming, Mn_3GaC displays several magnetic phase transitions: an AFM-intermediate (AFM-IM) phase transition at 160.1 K, an intermediate-FM (IM-FM) phase transition at 163.9 K, and a FM-paramagnetic (FM-PM) transition at 248 K[52]. As shown in Figure 2A, the determined magnetic moments m of AFM Mn_3GaC alternates along the [111] direction with a propagation vector $\boldsymbol{k}$ = (1/2, 1/2, 1/2), corresponding to m = 1.8 ± 0.1 μ_B/Mn at 4.2 K reported by Fruchart *et al.* and m = 1.54 μ_B/Mn at 150 K revealed by Çakır *et al.*[53-55]. As seen from Figure 2B, the propagation vector for FM

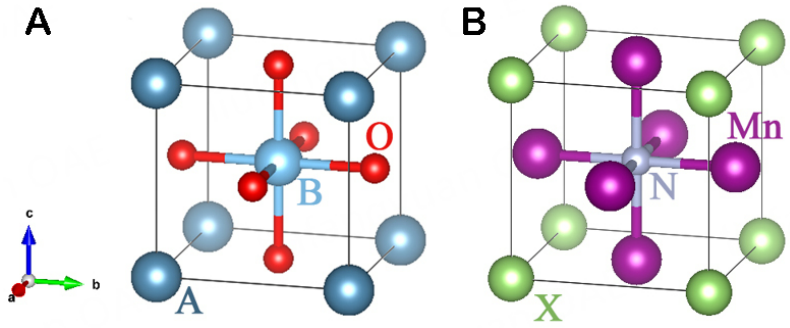

Figure 1. (A) Perovskite structure ABO_3; (B) antiperovskite structure Mn_3XN.

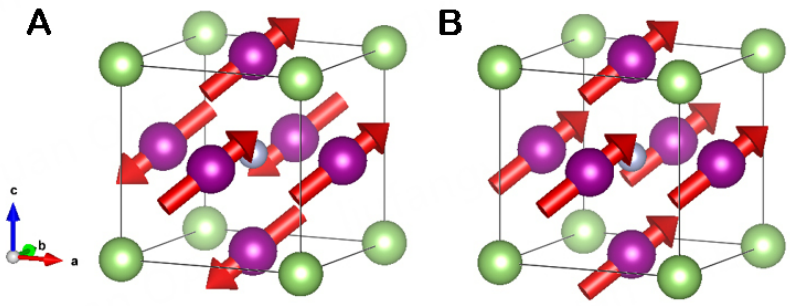

Figure 2. The collinear (A) AFM structure and (B) FM structure of Mn_3GaC.

Mn_3GaC is $\boldsymbol{k} = (0, 0, 0)$, displaying $m = 1.3 \pm 0.1$ μ_B/Mn at 193 K[53,54]. The direction [111] of easy magnetization is also confirmed by the Mössbauer effect[56].

Mn_3ZnN is characterized by two first-order magnetic transitions: PM-AFM at 183 K and AFM-AFM at 140 K. As shown in Figure 3A, the low temperature AFM phase is collinear within a $\sqrt{2}a, \sqrt{2}a, 2a$ sub-lattice of manganese, exhibiting two inequivalent magnetic atoms with different ordered magnetic moments[57]. The values of moments 0.61 μ_B on Mn1 (000) and 1.03 μ_B on Mn2 (1/4, 1/4, 1/4) were clarified by Fruchart *et al.*[58]. In 2012, we determined the ordered moments of 1.40 μ_B on Mn1 and 2.44 μ_B on Mn2 at 80 K for $Mn_3Zn_{0.99}N$ by neutron diffraction[20]. Moreover, for $Mn_{3.19}Zn_{0.77}N_{0.94}$, we observed a collinear FIM structure with a propagation vector $\boldsymbol{k} = (0, 0, 0)$ below 200 K [Figure 3B]. The magnetic moments alternate along the [111] direction with different values, corresponding to 0.5(1) (face-centered atom) and 1.3(7) (corner atom) μ_B/Mn for Mn atoms at 120 K[21].

Non-collinear magnetic structures

It is worth noting that two non-collinear AFM phases belonging to Γ^{4g} and Γ^{5g} types, respectively, have been studied extensively in antiperovskites. In this case, the compounds remain cubic with the propagation vector $\boldsymbol{k} = (0, 0, 0)$. For Γ^{5g} type shown in Figure 4A, the magnetic moments of Mn atoms are located in the (111) plane with a triangular arrangement. As seen from Figure 4B, the magnetic moments of Γ^{4g} are triangularly located in the (111) plane achieved by rotating 90° coherently from Γ^{5g} type. In Γ^{4g} and Γ^{5g} magnetic structures, two Mn atoms form an angle of 120° with each other in the (111) plane, and the magnetic moments of the three atoms cancel each other out to generate a zero net magnetic moment.

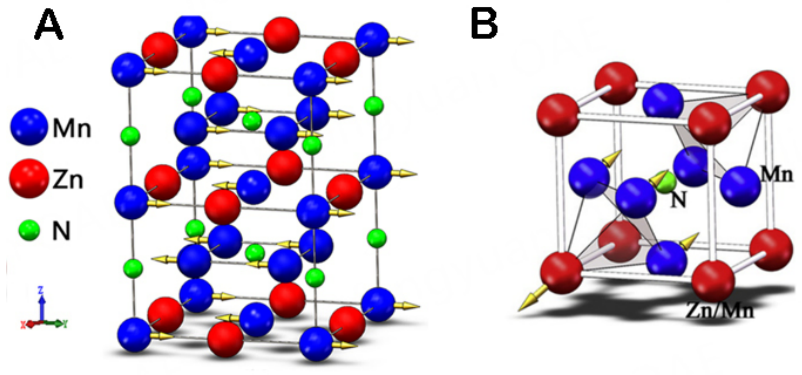

Figure 3. The collinear (A) AFM structure of Mn_3ZnN[57] and (B) the FIM structure of $Mn_{3.19}Zn_{0.77}N_{0.94}$[21].

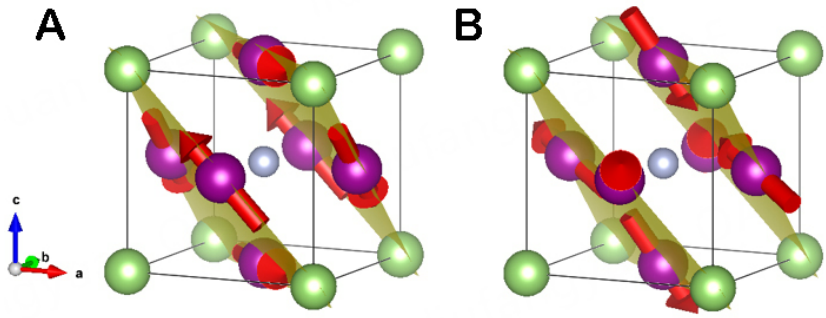

Figure 4. The non-collinear (A) Γ^{5g} and (B) Γ^{4g} AFM structures of antiperovskites.

So far, five typical undoped antiperovskites displaying the non-collinear magnetic structures of Γ^{4g} and Γ^{5g} types have been reported experimentally, including Mn_3NiN, Mn_3ZnN, Mn_3GaN, Mn_3AgN, and Mn_3SnN. The magnetic structure of Mn_3NiN below 163 K, Mn_3ZnN between 140 K and 183 K, Mn_3GaN below 298 K, and Mn_3AgN between 55 and 290 K belongs single-phase Γ^{5g} type, corresponding to the magnetic moments 0.98 μ_B/Mn (T = 77 K), 1.21 μ_B/Mn (T = 159 K), 1.17 μ_B/Mn (T = 4.2 K), and 3.1 μ_B/Mn (T = 4.2 K), respectively[54]. This type of magnetic structure has had an important impact on the mechanism exploration of the NTE behavior, piezomagnetic effect, and barocaloric effect of antiperovskites. In addition, the magnetic structures of Mn_3NiN between 163 K and 266 K, Mn_3AgN below 55 K and Mn_3SnN between 237 K and 357 K are composed of Γ^{4g} and Γ^{5g} types, showing the magnetic moments 0.8 μ_B/Mn at 250 K, 3.1 μ_B/Mn and 2.5 μ_B/Mn at 250 K at 4.2 K, respectively[54]. It was suggested that the magnetic behavior of antiperovskites is very sensitive to the differences of sample composition. In $Mn_3Ni_{0.9}N_{0.96}$, the magnetic structure is a combination of Γ^{4g} and Γ^{5g} symmetries below T_N = 264 K, and the moments undergo a rotation in the (111) plane upon warming[59]. Moreover, for $Mn_3Zn_{96}N$, the sample fully transforms to the Γ^{5g} phase upon cooling below 185 K, and the low-temperature collinear magnetic structure existing in Mn_3ZnN disappears[20].

The non-collinear Γ^{5g} AFM structure is also examined by both neutron diffraction and the correlated thermal expansion behavior in doped antiperovskites, such as $Mn_3Cu_{1-x}(Ge, Sn)_xN$, $Mn_3Zn_{1-x}(Ge, Sn)_xN$, and $Mn_3Ga_{1-x}Sn_xN$, *etc.*[5-22]. Particularly, the undoped Mn_3CuN does not display the Γ^{5g} magnetic configuration. As shown in Figure 5, a cubic structure with the Γ^{5g} magnetic configuration was determined by neutron study in $Mn_3Cu_{1-x}Ge_xN$ ($x \geq 0.15$), which is suggested to be a key ingredient of a large magnetovolume effect in antiperovskites[18]. Meanwhile, the NTE behavior determined by Γ^{5g} magnetic order was also observed in

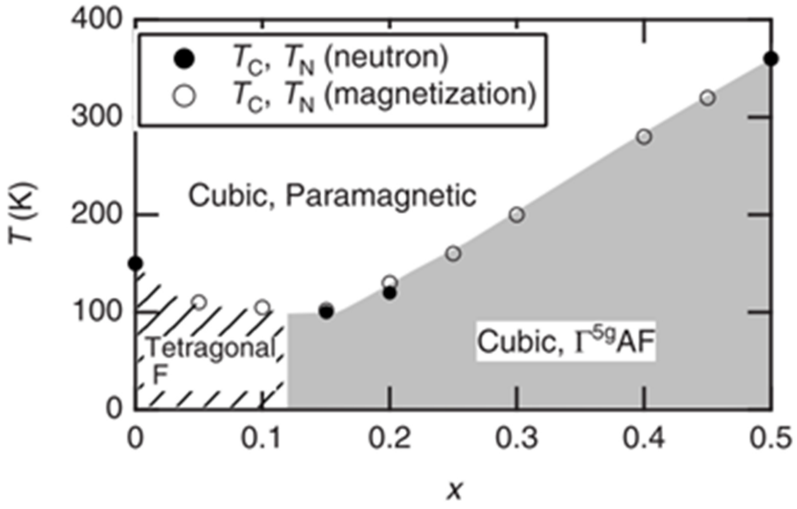

Figure 5. Phase diagram of $Mn_3Cu_{1-x}Ge_xN$. T_C and T_N denote the Curie and Néel temperatures, respectively[18].

$Mn_3Zn_{1-x}Ge_xN$[11,20]. In $Mn_3Cu_{1-x}Sn_xN$, the AFM transition closely coupled with the volume change is broadened upon Sn doping, producing the NTE behavior[19]. The characterization of magnetic structures in doped systems still requires careful study by neutron scattering.

Non-coplanar magnetic structures

A non-coplanar FIM structure with the propagation vector $\boldsymbol{k}$ = (1/2, 1/2, 0) has been reported in Mn_3CuN[54,60]. The magnetic ordering temperature of the Mn_3CuN compound is 143 K[54]. With cooling, the compound shows a transition from a high-temperature cubic phase to a low-temperature tetragonal phase. Herein, the magnetic moment direction of Mn atoms in the z = 0 plane is along the [001] direction, while the atoms in the z = 0.5 plane have two magnetic components, namely the FM arrangement in the [001] direction and the "square" AFM arrangement in the z = 0.5 plane[54]. It is worth noting that the antiperovskite Mn_3SnC with a magnetic ordering temperature of 294 K has the same type of magnetic structure as Mn_3CuN. Moreover, as shown in Figure 6A, an orthorhombic magnetic structure model with P_1 symmetry was determined in $Mn_3Cu_{0.89}N_{0.96}$. The sub-lattice of a magnetic structure is 2c × 2a × b, where a, b, and c are nuclear lattice parameters. At 6 K, neutron diffraction revealed that the Mn moments show an AFM component of 3.65 μ_B/Mn on the z = 0.5 plane and a FM component of 0.91 μ_B/Mn parallel to the y-axis on the x = 0.25 and 0.75 planes[39].

Figure 6B gives a non-collinear magnetic structure M-1 of $Mn_3Ga_{0.95}N_{0.94}$. The M-1 phase remains 79% in coexistence with Γ^{5g} magnetic configuration between 6 K and 50 K[35]. It can be seen that the sub-lattice of the M-1 phase is $\sqrt{2}a, \sqrt{2}a, a$, where a is the lattice parameter of the nuclear structure. For the M-1 phase, the results of neutron diffraction indicate that Mn atoms comprise three different locations, including Mn1 1a (0, 0, 0), Mn2 2b (0.5, 0.5, 0), and Mn3 4d (0.25, 0.25, 0.5). Mn1 and Mn2 display the AFM components along the z axis. Mn3 consists of two magnetic components; one is the "square" AFM component on the plane z = 0.5, and the other one is the FM component along a z axis direction. At 6 K, the AFM moment is 0.89 μ_B/Mn for Mn1 and Mn2, while Mn3 includes a FM moment of 2.18 μ_B/Mn and an AFM moment of 0.7 μ_B/Mn.

Recently, the non-collinear FIM structures were determined in the (1-x)Mn_3GaN- xMn_3SbN (0.2 ≤ x ≤ 0.8) heterogeneous system[61][Figure 6C]. Upon cooling, Mn_3SbN undergoes a PM-FIM phase transition at

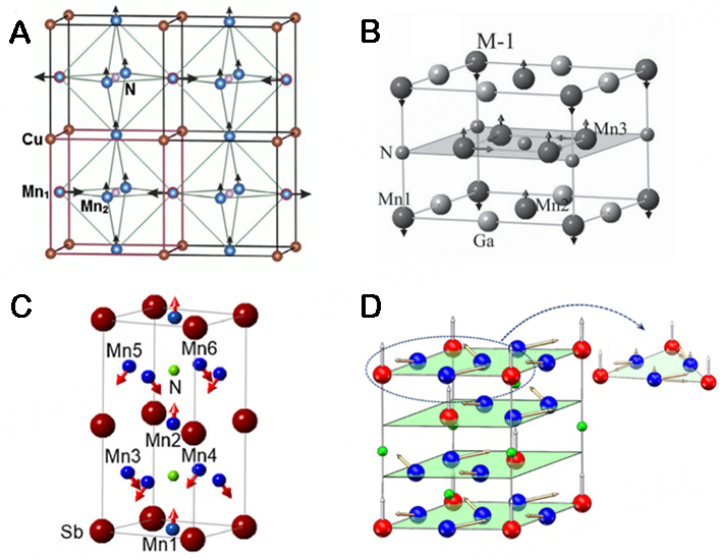

Figure 6. The non-coplanar FIM structures of (A) $Mn_3Cu_{0.89}N_{0.96}$ [39], (B) $Mn_3Ga_{0.95}N_{0.94}$ [35], (C) Mn_3SbN [61], and (D) $Mn_{3.39}Co_{0.61}N$ [62].

~353 K and FIM-M2 phase transition at ~250 K. Neutron diffraction pattern at 300 K reveals the non-collinear FIM phase with a sub-lattice *a*, *a*, 2*c* where a and c are the lattice parameters of the tetragonal nuclear structure. The Mn atoms are located at six different types of sites with a P4 space group. Mn1 (0.5, 0.5, 0) and Mn2 (0.5, 0.5, 0.5) display the FM component 2.5 μ_B/Mn along the z axis. Moreover, the tiled magnetic moments were uncovered for Mn3 (0.5, 0, 0.25), Mn4 (0, 0.5, 0.25), Mn5 (0.5, 0, 0.75), and Mn6 (0, 0.5, 0.75), corresponding to (−2.47, 2.47, −2.16) μ_B/Mn, (2.47, −2.47, −2.16) μ_B/Mn, (2.47, −2.47, −2.16) μ_B/Mn, and (−2.47, 2.47, −2.16) μ_B/Mn, respectively. At 5 K, another non-coplanar magnetic structure M2 with $\sqrt{2}a, \sqrt{2}a, a$ was revealed in Mn_3SbN. Herein, Mn atoms on the plane z = 0.5 show a "square" AFM arrangement with the moment 2.3 μ_B/Mn, while the other Mn atoms display the AFM component along the z axis with the moment 2.5 μ_B/Mn. The minor differences between the presented magnetic structure and the previously reported one may arise from the tiny elemental components[54]. Even more interesting in antiperovskites is that the propagation vector $\boldsymbol{k}$ = (0, 0, k_z) of Mn_3SnN varies with temperature from k_z = 0.25 at 50 K to k_z = 0.125 at 237 K[54].

The effect of magnetic element doping on the magnetic structure was also investigated in antiperovskites. For Mn-doped $Mn_{3+x}Ni_{1-x}N$ and $Mn_{3.39}Co_{0.61}N$ compounds [Figure 6D], a FM component along the [111] direction coexisting with canted Γ^{5g} AFM component was resolved by neutron diffraction technique[15,62]. Table 1 summarizes the magnetic structures and corresponding temperature ranges of typical antiperovskites.

PHYSICAL PROPERTIES OF ANTIPEROVSKITES

The research on antiperovskite structure compounds can be traced back to the 1930s when there were not many studies on physical properties. Since the 1980s, this type of compound has been paid attention by scientists, and the basic physical properties of antiperovskites have been studied by means of neutron diffraction, X-ray diffraction (XRD), Mössbauer spectroscopy, and nuclear magnetic resonance. Extensive research of these basic physical properties mainly includes crystal structures, magnetic properties (magnetic structures), phase diagrams, *etc.* At the beginning of the 21st century, superconductivity, giant magnetoresistance, magnetocaloric effect, abnormal thermal expansion, and near-zero temperature coefficient of resistance behaviors were successively reported in antiperovskites. The discovery of these physical properties prompted more and more researchers to pay attention to antiperovskites and their

Table 1. Magnetic structures and corresponding temperature ranges in antiperovskites

Antiperovskites	Magnetic ordering	Spin configurations	Temperature range
Mn_3GaC[52]	Ferromagnetic intermediate antiferromagnetic	Collinear	163.9 K < T < 248 K 160.1 K < T < 163.9 K T < 160.1 K
Mn3ZnN[58]	Antiferromagnetic	Γ^{5g} Collinear	140 K < T < 183 K T < 140 K
Mn_3NiN[54]	Antiferromagnetic	$\Gamma^{5g} + \Gamma^{4g}$ Γ^{5g}	163 K < T < 266 K T < 163 K
Mn_3GaN[54]	Antiferromagnetic	Γ^{5g}	T < 298 K
Mn_3AgN[54]	Antiferromagnetic	Γ^{5g} $\Gamma^{5g} + \Gamma^{4g}$	55 K <T < 290 K T < 55 K
Mn_3SnN[54]	Antiferromagnetic	Collinear $\Gamma^{5g} + \Gamma^{4g}$	357 K < T < 475 K 237 K < T< 357 K
Mn_3CuN[54]	Ferrimagnetic	Non-coplanar	T < 143 K

applications. In the past decade or so, a large number of physical properties correlated to magnetic structures have been reported.

Anomalous thermal expansion in manganese-based antiperovskites

Materials with zero thermal expansion (ZTE) and NTE behaviors have attracted widespread attention because of their broad applications in modern technology, such as high-precision optical instruments, microelectronics, aerospace devices, *etc.*[63-69]. A great deal of work has focused on the discovery of new materials and the improvement of thermal expansion properties. Nevertheless, the investigations for the mechanism of anomalous thermal expansion (ATE) (mainly including ZTE and NTE) are still needed. For ZrW_2O_8[67] and ScF_3[68], the mechanism associated with the soft phonon mode of the frame structure is adopted; moreover, the ATE behavior of the material has a strong coupling effect with other physical properties, such as the valence state change in $LaCu_3Fe_4O_{12}$[69], $BiNiO_3$[70], and YbGaGe[63] and the ferroelectric characteristics in $PbTiO_3$-$BiFeO_3$[71]; in addition, the ATE behavior emerges with magnetic transitions in various materials, such as the NTE in $La(Fe,Si,Co)_{13}$[72] and $Ca_2Ru_{1-x}Cr_xO_4$[73] and near ZTE in FeNi Invar[74] and $SrRuO_3$[75]. It is worth noting that although a large number of studies have shown that the Invar effect is related to the magnetic properties of materials, an adequate understanding of this property is still required. Therefore, the exploration of new materials with ATE will contribute to the clarification of mechanisms[75-80].

Some manganese nitrogen compounds (such as Mn_3ZnN at 185 K, Mn_3GaN at 298 K, *etc.*) are accompanied by a sudden change in volume during the magnetic transition, that is, the so-called magnetovolume effect. In 2005, Takenaka *et al.* reported the NTE behavior in the Ge-doped antiperovskite structure compound $Mn_3Cu_{1-x}Ge_xN$[5]. For Mn_3CuN, the compound itself has no magnetovolume effect. Through the doping of Ge, the discontinuous volume change caused by the magnetic volume effect is broadened, thereby realizing the regulation of the thermal expansion coefficient and temperature range of the NTE behavior. With increasing the doping amount of Ge, the magnetovolume effect of $Mn_3Cu_{1-x}Ge_xN$ was broadened and moved to the high temperature region, resulting in NTE behavior near room temperature. As shown in Figure 7A and 7B, near room temperature, the linear expansion coefficient α of $Mn_3Cu_{0.53}Ge_{0.47}N$ and $Mn_3Cu_{0.5}Ge_{0.5}N$ are -16×10^{-6} K^{-1} and -12×10^{-6} K^{-1}, respectively. In order to further reduce the material cost, Takenaka *et al.* used Sn as the dopant, which is cheaper than Ge. The doping of Sn can also broaden the NTE behavior of antiperovskites[6].

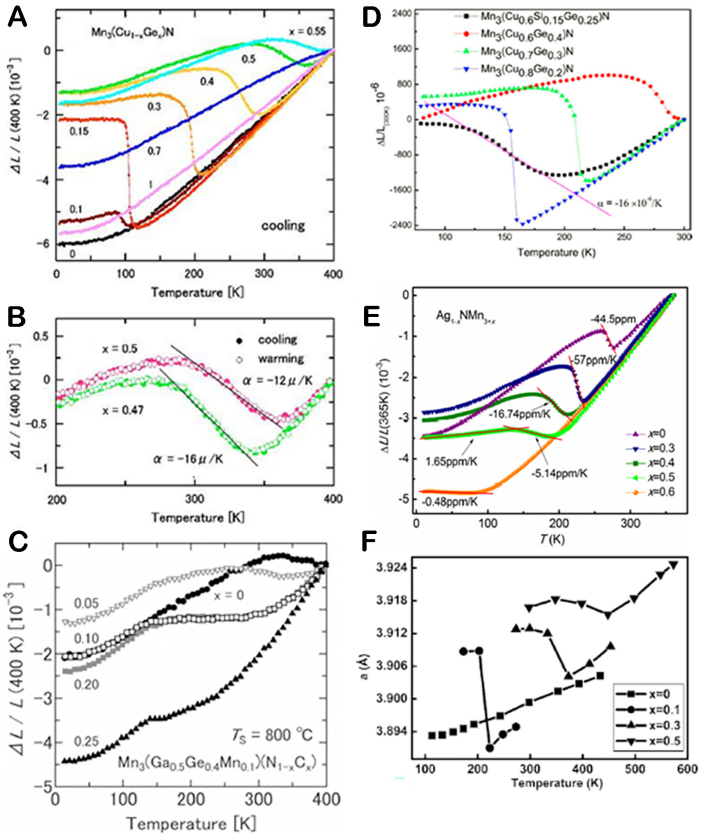

Figure 7. Linear thermal expansion of antiperovskites (A, B) $Mn_3Cu_{1-x}Ge_xN$[5],(C) $Mn_3Ga_{0.5}Ge_{0.4}Mn_{0.1}N_{1-x}C_x$[7],(D) $Mn_3Cu_{0.6}Si_xGe_{0.4-x}N$[8], (E) $Mn_{3+x}Ag_{1-x}N$[9], and (F) $Mn_3Zn_{1-x}Ge_xN$[11].

The thermal expansion behavior of $Mn_3Ga_{0.5}Ge_{0.4}Mn_{0.1}N_{1-x}C_x$ was also reported, and a single-phase ZTE material with a wider temperature range has been obtained[7]. As shown in Figure 7C, the thermal expansion behavior of $Mn_3Ga_{0.5}Ge_{0.4}Mn_{0.1}N_{1-x}C_x$ changes with the doping of C. When x = 0.1, the compound exhibits low thermal expansion in the temperature range of 190-272 K with $|\alpha| < 0.5 \times 10^{-6}$ K^{-1}. In addition, a very close correlation between N content and NTE behavior was found in $Mn_3Cu_{0.5}Sn_{0.5}N_{1-\delta}$. The N content in the compound decreases with the increase of the sintering temperature. When the sintering temperature is 950 degrees, the linear expansion coefficient of the compound with the N content of about 0.8 in the temperature range of 307-355 K with $|\alpha| < 0.5 \times 10^{-6}$ K^{-1}.

Huang *et al.* carried out research on Ge and Si co-doped $Mn_3Cu_{0.6}Si_xGe_{0.4-x}N$ and obtained a low-temperature NTE material[8]. As shown in Figure 7D, with the co-doping of Si, the NTE temperature range of the compound moves to a lower temperature. When x = 0.15, $Mn_3Cu_{0.6}Si_{0.15}Ge_{0.25}N$ shows NTE behavior in a wide temperature range in the temperature range of 120-184 K, and its linear expansion coefficient is $\alpha = -16 \times 10^{-6}$ K^{-1}. Comparing $Mn_3Cu_{0.6}Si_xGe_{0.4-x}N$ and $Mn_3Cu_{1-x}Ge_xN$, it can be seen that the single doping of Ge has a narrow volume mutation temperature range in the low temperature region (such as $Mn_3Cu_{0.8}Ge_{0.2}N$ around 155 K), while the co-doping of Si can make that the temperature range of the volume change of the compound is broadened and the behavior of NTE appears. The co-doping method provides a way to regulate the thermal expansion behavior of single-phase materials.

Lin *et al.* reported the thermal expansion and magnetic properties of antiperovskite manganese nitrides $Mn_{3+x}Ag_{1-x}N$[9]. The substitution of Mn for Ag effectively broadens the temperature range of NTE and moves

it to low temperatures [Figure 7E]. When x = 0.6, the $Mn_{3.6}Ag_{0.4}N$ compound shows ZTE with α = -0.48 × 10^{-6} K^{-1} (temperature range 5 - 87 K). Moreover, Lin *et al.* revealed a giant NTE covering room temperature in nanocrystalline Mn_3GaN_x[10]. By reducing the average grain size to ~10 nm, the temperature window ΔT for NTE exceeds 100 K, and α remains as large as -30 ppm/K (-21 ppm/K) for x = 1.0 (x = 0.9).

The influence of Ge and Sn doping on the thermal expansion behavior of $Mn_3Zn_{1-x}Ge(Sn)_xN$ has been investigated by us[11,12]. Figure 7F shows the variation of lattice constant with temperature in $Mn_3Zn_{1-x}Ge_xN$. The doping of Ge broadens the magnetovolume effect of $Mn_3Zn_{1-x}Ge_xN$ and moves the temperature zone to the higher one, thereby realizing the regulation of NTE behavior. A similar behavior was also observed in Sn-doped $Mn_3Zn_{1-x}Sn_xN$ compounds[12]. On the other hand, the regulation of the thermal expansion behavior of Mn_3NiN-based compounds has also been reported[13,14]. Antiperovskite $Mn_3Ni_{0.5}Ag_{0.5}N$ shows NTE behavior in a wide temperature range (260-320 K) near room temperature with α = -12 × 10^{-6} K^{-1}. The $Mn_3Ni_{0.5}Cu_{0.5}N$ exhibits NTE in the temperature range of 160-240 K (ΔT = 80 K) with α = -22.3 × 10^{-6} K^{-1}. Interestingly, a new type of Invar-like material exhibiting ZTE has been revealed in $Mn_{3+x}Ni_{1-x}N$[15].

Song *et al.* revealed the ZTE behavior of $Mn_3Cu_{0.5}Ge_{0.5}N$ due to the size effect[16]. When $Mn_3Cu_{0.5}Ge_{0.5}N$ was prepared from polycrystalline samples (average size of 2.0 μm) to ultra-nanocrystals (average size of 12 nm), the occupancy rate of Mn in the sample changed from 100% to 78.7% [Figure 8A]. Meanwhile, the ultra-nanocrystalline sample exhibits ZTE behavior in a wide temperature range ΔT = 218 K (12-230 K) with α = 1.18 × 10^{-7} K^{-1}.

The mechanism for the NTE of antiperovskites was investigated by Iikub *et al.* The neutron diffraction results indicate that the non-collinear Γ^{5g} AFM structure plays a key role in the magnetovolume effect of $Mn_3Cu_{1-x}Ge_xN$, which leads to the appearance of NTE behavior. Moreover, Iikub *et al.* further revealed that the local lattice distortion plays a very important role in the NTE of $Mn_3Cu_{1-x}Ge_xN$[17] [Figure 8B]. As suggested by the pair distribution function (PDF) analysis, $Mn_3Cu_{1-x}Ge_xN$ maintains a cubic structure within a certain doping range, while the Mn_6N octahedrons in $Mn_3Cu_{1-x}Ge_xN$ rotate along the z-axis with Ge doping to form a local lattice distortion. This structural instability displays a strong correlation with the broadness of the growth of the ordered magnetic moment, which is considered as a trigger for broadening the volume change[18]. Moreover, Tong *et al.* studied the magnetic transition broadening and local lattice distortion in $Mn_3Cu_{1-x}Sn_xN$ with NTE[19]. The PDF results indicate that the distribution of Cu/Sn-Mn bonds is linked to the fluctuations of the AFM integral. This may account for the broadening of the volume change in antiperovskites.

Through the study of $Mn_3(Zn, M)_xN$(M = Ag, Ge), we revealed the quantitative relationship between thermal expansion and atomic magnetic moments in antiperovskites and realized the regulation of thermal expansion[20]. A collinear AFM structure M_{PTE} and a non-collinear AFM structure Γ^{5g} are observed in Mn_3Zn_xN. Herein, the M_{PTE} phase displays PTE behavior, while the Γ^{5g} configuration shows NTE behavior. The NTE of Γ^{5g} phase can balance the contributions from PTE generated by the anharmonic vibration in the sample, producing the ZTE of antiperovskites. By introducing vacancies into Mn_3Zn_xN, the existence of a temperature range for Γ^{5g} configuration can be effectively regulated, thereby obtaining a ZTE material with a wider temperature range. In addition, we also discussed the quantitative relationship between the anomalous change of the lattice and the atomic magnetic moments for the Γ^{5g} phase. As shown in Figure 8C, both the lattice change a_{NTE} - a_T and the atomic magnetic moment m in Mn_3Zn_xN gradually decrease with the increase of temperature, and the change trends for both factors are consistent. By defining r(T) = (a_{NTE} - a_T)/m, it is obtained that r(T) hardly changes with temperature where a_{NTE}, a_T and m are the lattice constants and magnitude of the ordered magnetic moment, which confirms that there is a strong

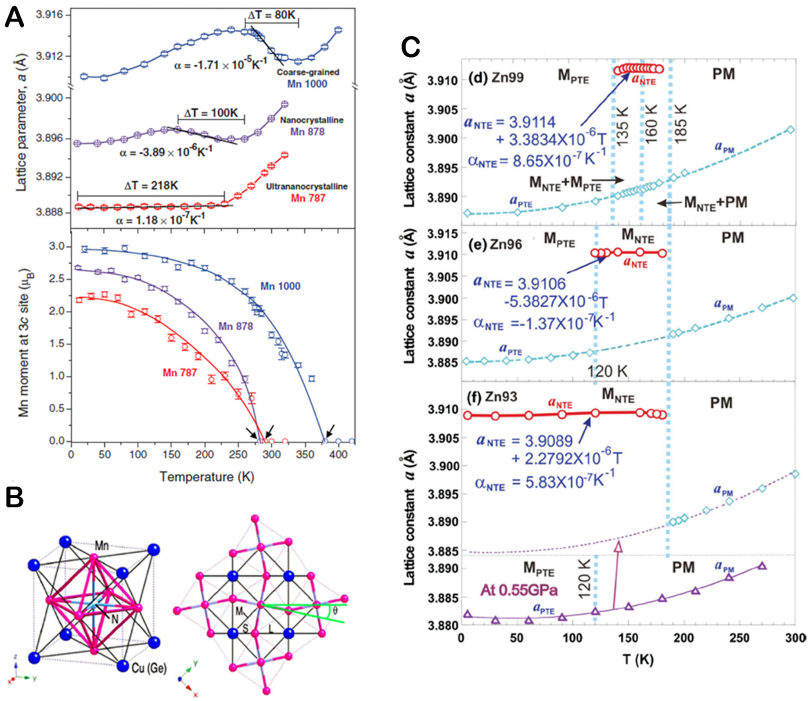

Figure 8. (A) ZTE behavior of $Mn_3Cu_{0.5}Ge_{0.5}N$[16]; (B) local lattice distortion of $Mn_3Cu_{1-x}Ge_xN$[17]; (C) the relationship between the anomalous change of the lattice and the atomic magnetic moments for Γ^{5g} phase of Mn_3Zn_xN[20].

spin-lattice coupling between the lattice constant and the atomic magnetic moment in Mn_3Zn_xN. In addition, the strong spin-lattice coupling that can be tuned to achieve ZTE behavior was further confirmed in antiperovskite $Mn_{3+x}Ni_{1-x}N$ and $Mn_{3.19}Zn_{0.77}N_{0.94}$ within Γ^{5g} phase[15,21]. Meanwhile, in $Mn_3Ga_{1-x}Sn_xN$ with Γ^{5g} phase, the increase of the phonon contribution to the thermal expansion induced by Sn doping and the corresponding decrease of dm/dT are revealed to be the key parameters for tuning the magnetovolume effect[22].

The first-principle calculations have been adopted for understanding the NTE behavior of antiperovskites. The primary theoretical works focus on the comparison of differences in equilibrium volumes of antiperovskites with different magnetic structures. Lukashev *et al.* found that the equilibrium volume of the Γ^{5g} AFM state in Mn_3GaN is larger than that of the PM state, which confirms that the magnetic transition in the material can lead to volume change (magnetovolume effect)[23]. Qu *et al.* calculated the energy-lattice curves of various magnetic configurations, and the results show that the Γ^{5g} AFM state has the largest volume. This work also confirms that the Γ^{5g} AFM state has the largest volume compared to other magnetic configurations[24]. In addition, Mochizuki *et al.* constructed a classical spin model with frustrated exchange interactions and magnetic anisotropy to study the nontrivial magnetic orders in the antiperovskite Mn_3AN. With a replica-exchange Monte Carlo technique, the Γ^{5g} and Γ^{4g} spin configurations, known to trigger the NTE, have been reproduced[25].

Electronic transport properties in antiperovskites

There is a strong correlation between the lattice, spin, and charge of Mn_3GaC. Therefore, a giant magnetoresistance effect was found near its collinear AFM - collinear FM magnetic transition[26]. The size of magnetoresistance can be expressed by $[\rho(H) - \rho(0)]/\rho(0)$, and $\rho(H)$ and $\rho(0)$ represent the resistivity when the external magnetic field is finite and 0, respectively. As shown in Figure 9A, Mn_3GaC generates a

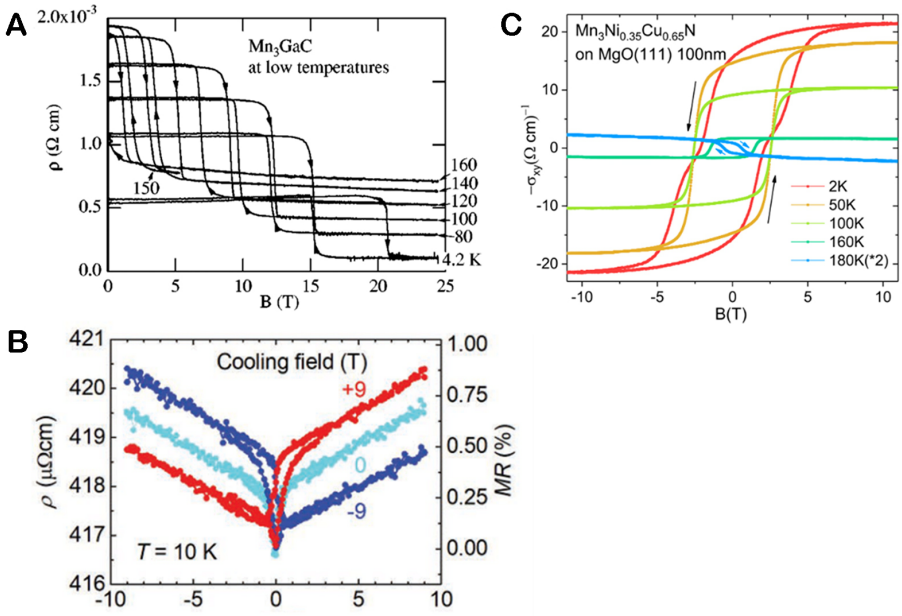

Figure 9. (A) Giant magnetoresistance effect of Mn_3GaC at selected temperatures[26]; (B) magnetoresistance of $Mn_{3.338}Ni_{0.651}N$ after cooling in zero field and in ±9 T[27]; (C) anomalous Hall conductivity versus field measured in single crystalline $Mn_3Ni_{0.35}Cu_{0.65}N$ film on MgO (111) substrate[30].

magnetoresistance of about 50% under an external magnetic field of 3 kOe. With the further increase of the external magnetic field, the magnetoresistance value is almost unchanged, but its peak width is broadened and reaches 20 K at 50 kOe. Kamishima *et al.* suggested that the magnetoresistance effect in Mn_3GaC is aroused by the difference of resistivity between AFM and FM states, and the external magnetic field can induce the temperature shift of AFM-FM phase transition[26]. In addition, an electroresistance-like behavior of the antiperovskite Mn_3GaC, revealed by a resistivity change of 50% due to the local Joule heating, is reported around the collinear AFM- intermediate phase transition. The currents significantly reduce the proportion of the higher resistivity AFM phase relative to the lower resistivity interphase with warming, showing a change in resistivity. On the other hand, for a non-coplanar magnet $Mn_{3.338}Ni_{0.651}N$ with triangular lattice, a high-resistivity state can be frozen along the direction of the cooling field while a low-resistivity state is determined in the reversed field direction, indicating an asymmetry with respect to H [Figure 9B]. This characteristic further demonstrates a switchable scalar spin chirality of $Mn_{3.338}Ni_{0.651}N$.

Recently, the anomalous Hall effect, originating from the nonvanishing momentum space Berry curvature, has been reported in the non-collinear AFM antiperovskites. Among the magnetic orders, a typical non-collinear AFM configuration is Γ^{4g}, whose atomic magnetic moments point to the triangle "inside" or "outside" in the triangular lattice of the antiperovskite (111) surface, forming a phase similar to that of Mn_3A(X = Sn, Ge, Pt) non-collinear magnets. Another typical AFM phase Γ^{5g} can be obtained by rotating the atomic magnetic moments in Γ^{4g} by 90 degrees in the (111) plane. Both of these two magnetic phases have zero scalar chirality, and theoretical studies show that the former and the latter magnetic order display a finite and zero anomalous Hall resistivity, respectively. In 2019, Gurung *et al.* used symmetry analysis and density functional theory to study the anomalous Hall conductance in non-collinear magnetic antiperovskites, revealing that the Γ^{4g} magnetic phase in Mn_3GaN shows a finite value of anomalous Hall conductivity, while the Γ^{5g} magnetic phase displays zero anomalous Hall conductivity[28]. In 2020, Samathrakis *et al.* theoretically calculated the tailoring of the anomalous Hall effect in the non-collinear antiperovskite Mn_3GaN, revealing the large intrinsic anomalous Hall effect caused by the strain in the Γ^{5g}

and Γ^{4g} magnetic phases[29]. In 2019, Zhao *et al.* experimentally observed the anomalous Hall effect in the non-collinear AFM $Mn_3Ni_{1-x}Cu_xN$, which is attributed to the nonzero Berry curvature of the Γ^{4g} magnetic phase in momentum space [Figure 9C][30]. The research on the anomalous Hall effect of antiperovskites is attracting widespread attention for novel spintronic applications.

Piezomagnetic/baromagnetic effects in antiperovskites

The piezomagnetic effect has been reported in non-collinear AFM antiperovskites[23,33]. In 2008, Lukashev *et al.* predicted that the non-collinear magnetic structure of Mn_3GaN can be controlled by a small applied biaxial strain [Figure 10A][23]. Figure 10B shows the net magnetic moment of Mn_3GaN and the rotational angle of the magnetic moment of Mn atoms as a function of axial strain. It can be seen that the atomic magnetic moment rotates when the strain is applied. This piezomagnetic effect is linear and displays magnetization reversal with the applied strain. As the compressive strain is 1%, the magnetization is about 0.04 μ_B/f.u. Therefore, this property can be utilized for the application of the magnetoelectric effect, such as a combination of piezomagnetic and piezoelectric phases or a combination of magnetostrictive and piezoelectric phases[31,32]. In addition, Zemen *et al.* theoretically performed a systematic study of the piezomagnetic effect in nine cubic antiperovskites Mn_3XN (X = Rh, Pd, Ag, Co, Ni, Zn, Ga, In, Sn), revealing an extraordinarily large piezomagnetic effect in Mn_3SnN at room temperature[33]. Boldrin *et al.* demonstrate experimentally that a giant piezomagnetic effect is indeed manifest in the AFM antiperovskite Mn_3NiN[34].

In 2016, the baromagnetic effect of $Mn_3Ga_{0.95}N_{0.94}$ was determined by both neutron diffraction analysis and magnetic measurements[35]. Interestingly, $Mn_3Ga_{0.95}N_{0.94}$ displays a new tetragonal non-coplanar magnetic structure M-1 below 50 K, which is in coexistence with Γ^{5g} spin configuration under atmospheric pressure. As shown in Figure 10C and D, the sample exhibits the piezomagnetic effect. When the applied pressure is 750 MPa at 130 K, the magnetic phase transition from M-1 to Γ^{5g} AFM appears, generating the piezomagnetic characteristic of 0.63 μ_B/f.u. Combined with the refined results of neutron diffraction, the change of Mn-Mn distance and spin rearrangement caused by pressure is considered to be the trigger of the observed baromagnetic effect.

Magnetocaloric effect

The magnetocaloric effect of antiperovskites was primarily reported in Mn_3GaC[36]. The collinear AFM-intermediate magnetic transition of Mn_3GaC showing a first-order characteristic can be controlled by an external magnetic field, generating the magnetocaloric effect. Figure 11A shows the temperature dependence of the maximum value of magnetic entropy change ΔS_{mag}. The peak of ΔS_{mag} reaches 17 J/(kg·K) when the external magnetic field is 10 kOe, and the peak value broadens to a "platform" shape with further increase of the magnetic field. In addition, by introducing C vacancies, the magnetic properties of Mn_3GaC were changed, thereby affecting the magnetocaloric effect[37]. The magnetic entropy of $Mn_3GaC_{0.78}$ decreased to 3.7 J/kg·K under a 5 T magnetic field. In $Mn_{3-x}Co_xGaC$, Co doping can reduce the first-order phase transition temperature from 164 K to 100 K without a significant decrease of magnetic entropy and realize the magnetocaloric effect covering a wider temperature range (50-160 K)[38].

A large magnetic entropy change was observed in $Mn_3Cu_{0.89}N_{0.96}$[39] [Figure 11B]. By introducing vacancies, the onset of the FIM-PM transition is slightly reduced from 150 K of Mn_3CuN to 147.7 K of $Mn_3Cu_{0.89}N_{0.96}$, and a new non-coplanar FIM structure with an orthorhombic symmetry was determined. The total entropy change of $Mn_3Cu_{0.89}N_{0.96}$ obtained by DSC is about 60 J/kg·K, while the maximum magnetic entropy change ΔS_{mag} is 13.52 J/kg·K under a magnetic field of 50 kOe near the temperature of FIM-PM transition. Neutron diffraction results indicate that the magnetic entropy change of $Mn_3Cu_{0.89}N_{0.96}$ is caused by the magnetic transition from the AFM to the FM component in the tetragonal phase and the phase transition from cubic to tetragonal under a magnetic field.

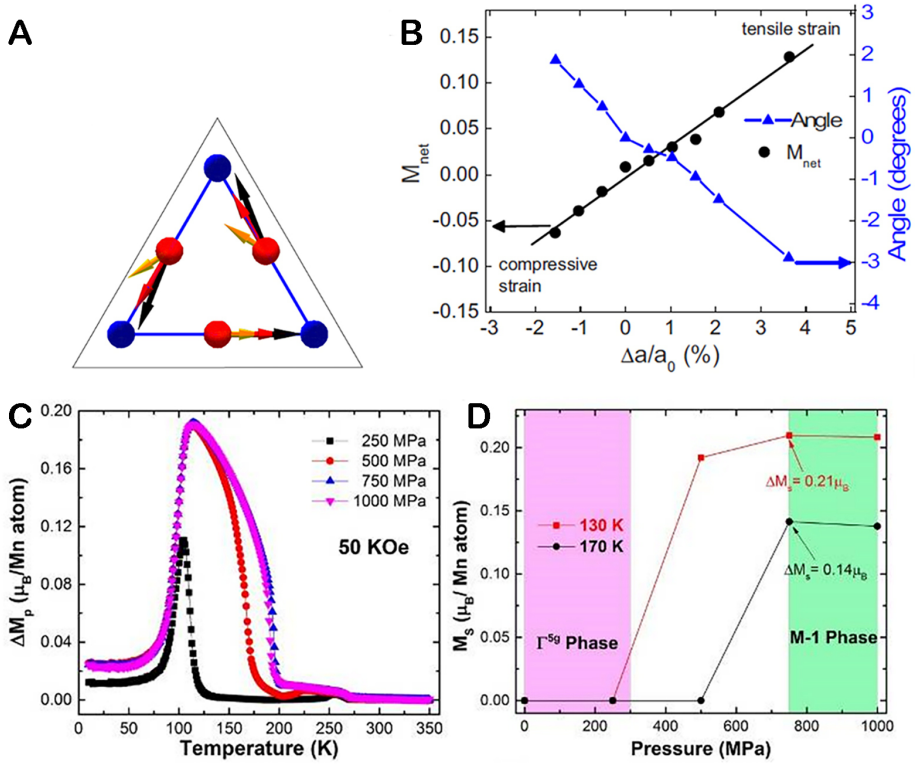

Figure 10. (A) Variation of magnetic moment of Mn Atoms in the (111) Plane of Γ^{5g} AFM Mn_3GaN with axial strain[23]; (B) variation of net magnetic moment and rotation angle of Mn atomic magnetic moment with axial strain for Mn_3GaN[23]; (C) piezomagnetic effect determined by magnetization curve in $Mn_3Ga_{0.95}N_{0.94}$[35]; (D) piezomagnetic effect of in $Mn_3Ga_{0.95}N_{0.94}$ at 130 K and 170 K[35].

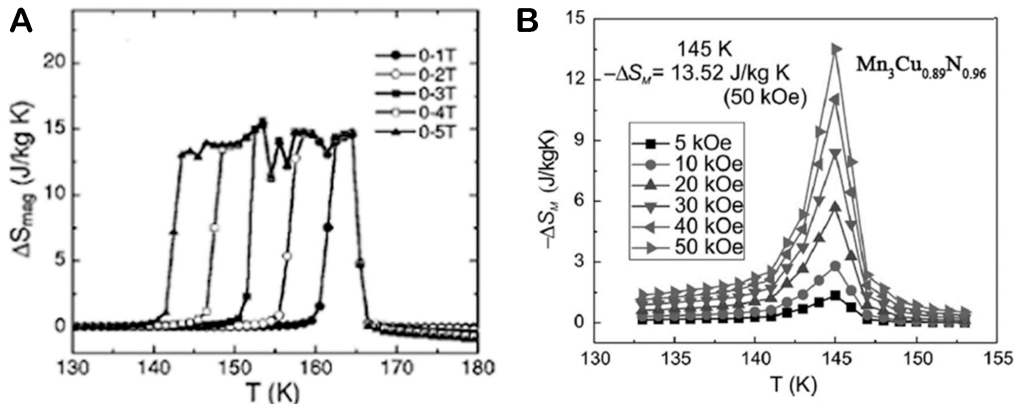

Figure 11. Magnetocaloric effect of (A) Mn_3GaC[36] and (B) $Mn_3Cu_{0.89}N_{0.96}$[39].

Barocaloric effect

A significant barocaloric effect is expected when strong cross-correlations between the volume and magnetic order appear in materials. In 2015, Matsunami *et al.* reported the giant barocaloric effect enhanced by the frustration of the AFM phase in Mn_3GaN[40]. As shown in Figure 12A, when a hydrostatic pressure change of 139 MPa is applied, Mn_3GaN exhibits an entropy change of 22.3 J kg^{-1} K^{-1}. By applying a depressurization of 93 MPa, the change of adiabatic temperature is determined to be about 5 K.

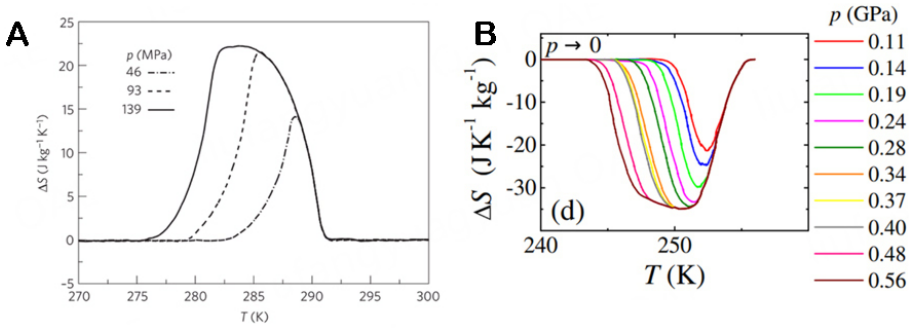

Figure 12. (A) The entropy change of Mn_3GaN under different hydrostatic pressures as a function of temperature[40]; (B) isothermal entropy and adiabatic temperature changes[41].

Matsunami *et al.* further suggests that the magnitude of the barocaloric effect of Mn_3GaN is determined by the volume change at the transition and stability of the AFM phase against the pressure[40]. In 2018, Boldrin *et al.* further investigated the barocaloric effect in the geometrically frustrated antiferromagnet Mn_3NiN [Figure 12B][41]. It is worth noting that a large barocaloric entropy change, which is a factor of 1.6 than that of Mn_3GaN, is observed. Boldrin *et al.* proposed that the barocaloric effect of Mn_3NiN originates from multisite exchange interactions amongst the local Mn magnetic moments and their coupling with itinerant electron spins[41].

CONCLUSION AND OUTLOOK

As reviewed in this article, owing to the magnetic frustration prompted by Mn_6N or Mn_6C octahedra, antiperovskites display the abounding magnetic structures, including collinear AFM, collinear FM, collinear FIM, non-collinear magnetic and non-coplanar magnetic spin configurations. In antiperovskites, the magnetic phase transition (magnetic structures), abnormal lattice change, and electronic transport properties are interrelated and affect each other, showing a large number of physical properties such as ATE, electronic transport properties, piezomagnetic/baromagnetic effects, magnetocaloric effect, barocaloric effect, *etc*. Therefore, antiperovskites will be an excellent candidate for exploring new smart materials. In order to further optimize performance and explore mechanisms, the following issues for in-depth research deserve attention and solutions:

Exploration of new magnetic structures. The examination of new physical properties is one of the important directions of the development of modern smart materials. Due to the strong correlation of "lattice-spin-charge", antiperovskites show a series of rich and unique physical properties within some specific magnetic structures. Although the determination of the magnetic structures is a central issue in antiperovskites, there is still a lack of systematic and in-depth research, especially on how the magnetic structures and correlated physical properties evolve in the case of elemental doping, variated temperatures, varied magnetic fields, and pressurization.

Synthesis of single crystal samples. The current research work on antiperovskites is mainly focused on polycrystalline. From the perspective of mechanism research and application, single crystal research has greater advantages. However, it is difficult to precisely control the nitrogen/carbon contents of antiperovskites in preparation, and the change of contents has a great influence on its physical properties. Therefore, the synthesis of three-dimensional single crystal materials with excellent physical properties is challenging.

Practical application research. Selecting some typical antiperovskites with fascinating physical properties, the practical applications can be explored in the fields of optics, microelectronics, refrigeration, aerospace, *etc*.

DECLARATIONS

Authors' contributions

Conceived and designed the manuscript: Deng S, He L, Wang C
Drafted and revised the manuscript: Deng S, Wang H, He L, Wang C

Availability of data and materials

Not applicable.

Financial support and sponsorship

This work was financially supported by the Guangdong Basic and Applied Basic Research Foundation (2022A1515140117), Large Scientific Facility Open Subject of Songshan Lake (Dongguan, Guangdong), the National Key R&D Program of China (Grant No. 2021YFA1600602 and No. 2021YFA1600603) and National Natural Science Foundation of China (Grant No. 52371190, No. U2032167, No. 12041202, No. U2032220, No. U1832219, and No. 52272264), the Sino-German Mobility Programme (No. M-0273), and the Key Program of the Chinese Academy of Sciences (CAS).

Conflicts of interest

All authors declared that there are no conflicts of interest.

Ethical approval and consent to participate

Not applicable.

Consent for publication

Not applicable.

REFERENCES

1. Bednorz JG, Müller KA. Possible highT c superconductivity the Ba-La-Cu-O system. *Z Physik B Condens Matter* 1986;64:189-93. DOI
2. Ahn CH, Tybell T, Antognazza L, et al. Local, nonvolatile electronic writing of epitaxial $Pb(Zr_{0.52}Ti_{0.48})O_3/SrRuO_3$ heterostructures. *Science* 1997;276:1100-3. DOI
3. von Helmolt R, Wecker J, Holzapfel B, Schultz L, Samwer K. Giant negative magnetoresistance in perovskitelike $La_{2/3}Ba_{1/3}MnO_x$ ferromagnetic films. *Phys Rev Lett* 1993;71:2331-3. DOI PubMed
4. Chen J, Nittala K, Forrester JS, et al. The role of spontaneous polarization in the negative thermal expansion of tetragonal $PbTiO_3$-based compounds. *J Am Chem Soc* 2011;133:11114-7. DOI
5. Takenaka K, Takagi H. Giant negative thermal expansion in Ge-doped anti-perovskite manganese nitrides. *Appl Phys Lett* 2005;87:261902. DOI
6. Takenaka K, Asano K, Misawa M, Takagi H. Negative thermal expansion in Ge-free antiperovskite manganese nitrides: Tin-doping effect. *Appl Phys Lett* 2008;92:011927. DOI
7. Takenaka K, Takagi H. Zero thermal expansion in a pure-form antiperovskite manganese nitride. *Appl Phys Lett* 2009;94:131904. DOI
8. Huang R, Li L, Cai F, Xu X, Qian L. Low-temperature negative thermal expansion of the antiperovskite manganese nitride Mn_3CuN codoped with Ge and Si. *Appl Phys Lett* 2008;93:081902. DOI
9. Lin JC, Tong P, Tong W, et al. Tunable negative thermal expansion related with the gradual evolution of antiferromagnetic ordering in antiperovskite manganese nitrides $Mn_{3+x}Ag_{1-x}N$ ($0 \le x \le 0.6$). *Appl Phys Lett* 2015;106:082405. DOI

10. Lin JC, Tong P, Zhou XJ, et al. Giant negative thermal expansion covering room temperature in nanocrystalline GaN_xMn_3. *Appl Phys Lett* 2015;107:131902. DOI
11. Sun Y, Wang C, Wen Y, Zhu K, Zhao J. Lattice contraction and magnetic and electronic transport properties of $Mn_3Zn_{1-x}GexN$. *Appl Phys Lett* 2007;91:231913. DOI
12. Sun Y, Wang C, Wen Y, et al. Negative thermal expansion and magnetic transition in anti-perovskite structured $Mn_3Zn_{1-x}Sn_xN$ compounds: rapid communications of the American ceramic society. *J Am Ceram Soc* 2010;93:2178-81. DOI
13. Ding L, Wang C, Sun Y, Colin CV, Chu L. Spin-glass-like behavior and negative thermal expansion in antiperovskite $Mn_3Ni_{1-x}Cu_xN$ compounds. *J Appl Phys* 2015;117:213915. DOI
14. Chu L, Wang C, Yan J, et al. Magnetic transition, lattice variation and electronic transport properties of Ag-doped $Mn_3Ni_{1-x}Ag_xN$ antiperovskite compounds. *Scr Mater* 2012;67:173-6. DOI
15. Deng S, Sun Y, Wu H, et al. Invar-like behavior of antiperovskite $Mn_{3+x}Ni_{1-x}N$ compounds. *Chem Mater* 2015;27:2495-501. DOI
16. Song X, Sun Z, Huang Q, et al. Adjustable zero thermal expansion in antiperovskite manganese nitride. *Adv Mater* 2011;23:4690-4. DOI
17. Iikubo S, Kodama K, Takenaka K, Takagi H, Takigawa M, Shamoto S. Local lattice distortion in the giant negative thermal expansion material $Mn_3Cu_{1-x}Ge_xN$. *Phys Rev Lett* 2008;101:205901. DOI PubMed
18. Iikubo S, Kodama K, Takenaka K, Takagi H, Shamoto S. Magnetovolume effect in $Mn_3Cu_{1-x}Ge_xN$ related to the magnetic structure: neutron powder diffraction measurements. *Phys Rev B* 2008;77:020409. DOI
19. Tong P, Louca D, King G, Llobet A, Lin JC, Sun YP. Magnetic transition broadening and local lattice distortion in the negative thermal expansion antiperovskite $Cu_{1-x}Sn_xNMn_3$. *Appl Phys Lett* 2013;102:041908. DOI
20. Wang C, Chu L, Yao Q, et al. Tuning the range, magnitude, and sign of the thermal expansion in intermetallic Mn_3 (Zn, *M*)*x* N(*M* = Ag, Ge). *Phys Rev B* 2012;85:220103. DOI
21. Deng S, Sun Y, Wu H, et al. Phase separation and zero thermal expansion in antiperovskite $Mn_3Zn_{0.77}Mn_{0.19}N_{0.94}$: an in situ neutron diffraction investigation. *Scr Mater* 2018;146:18-21. DOI
22. Shi K, Sun Y, Colin CV, et al. Investigation of the spin-lattice coupling in $Mn_3Ga_{1-x}Sn_xN$ antiperovskites. *Phys Rev B* 2018;97:054110. DOI
23. Lukashev P, Sabirianov RF, Belashchenko K. Theory of the piezomagnetic effect in Mn-based antiperovskites. *Phys Rev B* 2008;78:184414. DOI
24. Qu BY, Pan BC. Nature of the negative thermal expansion in antiperovskite compound Mn_3ZnN. *J Appl Phys* 2010;108:113920. DOI
25. Mochizuki M, Kobayashi M, Okabe R, Yamamoto D. Spin model for nontrivial types of magnetic order in inverse-perovskite antiferromagnets. *Phys Rev B* 2018;97:060401. DOI
26. Kamishima K, Goto T, Nakagawa H, et al. Giant magnetoresistance in the intermetallic compound Mn_3GaC. *Phys Rev B* 2000;63:024426. DOI
27. Deng S, Fischer G, Uhlarz M, et al. Controlling chiral spin states of a triangular-lattice magnet by cooling in a magnetic field. *Adv Funct Mater* 2019;29:1900947. DOI
28. Gurung G, Shao DF, Paudel TR, Tsymbal EY. Anomalous HALL conductivity of noncollinear magnetic antiperovskites. *Phys Rev Mater* 2019;3:044409. DOI
29. Samathrakis I, Zhang H. Tailoring the anomalous Hall effect in the noncollinear antiperovskite Mn_3GaN. *Phys Rev B* 2020;101:214423. DOI
30. Zhao K, Hajiri T, Chen H, Miki R, Asano H, Gegenwart P. Anomalous Hall effect in the noncollinear antiferromagnetic antiperovskite $Mn_3Ni_{1-x}Cu_xN$. *Phys Rev B* 2019;100:045109. DOI
31. Rani GM, Wu CM, Motora KG, Umapathi R. Waste-to-energy: utilization of recycled waste materials to fabricate triboelectric nanogenerator for mechanical energy harvesting. *J Clean Prod* 2022;363:132532. DOI
32. Gokana MR, Wu CM, Motora KG, Qi JY, Yen WT. Effects of patterned electrode on near infrared light-triggered cesium tungsten bronze/ poly(vinylidene)fluoride nanocomposite-based pyroelectric nanogenerator for energy harvesting. *J Power Sources* 2022;536:231524. DOI
33. Zemen J, Gercsi Z, Sandeman KG. Piezomagnetism as a counterpart of the magnetovolume effect in magnetically frustrated Mn-based antiperovskite nitrides. *Phys Rev B* 2017;96:024451. DOI
34. Boldrin D, Mihai AP, Zou B, et al. Giant Piezomagnetism in Mn_3NiN. *ACS Appl Mater Interfaces* 2018;10:18863-8. DOI
35. Shi K, Sun Y, Yan J, et al. Baromagnetic effect in antiperovskite $Mn_3Ga_{0.95}N_{0.94}$ by neutron powder diffraction analysis. *Adv Mater* 2016;28:3761-7. DOI
36. Tohei T, Wada H, Kanomata T. Negative magnetocaloric effect at the antiferromagnetic to ferromagnetic transition of Mn_3GaC. *J Appl Phys* 2003;94:1800-2. DOI
37. Yu M, Lewis LH, Moodenbaugh AR. Assessment of the magnetic entropy change in the metallic antiperovskite $Mn_3GaC_{1-\delta}$ (δ = 0, 0.22). *J Magn Magn Mater* 2006;299:317-26. DOI
38. Tohei T, Wada H, Kanomata T. Large magnetocaloric effect of $Mn_{3-x}Co_xGaC$. *J Magn Magn Mater* 2004;272-76:E585-6. DOI
39. Yan J, Sun Y, Wu H, et al. Phase transitions and magnetocaloric effect in $Mn_3Cu_{0.89}N_{0.96}$. *Acta Mater* 2014;74:58-65. DOI
40. Matsunami D, Fujita A, Takenaka K, Kano M. Giant barocaloric effect enhanced by the frustration of the antiferromagnetic phase in Mn_3GaN. *Nat Mater* 2015;14:73-8. DOI PubMed
41. Boldrin D, Mendive-tapia E, Zemen J, et al. Multisite exchange-enhanced barocaloric response in Mn_3NiN. *Phys Rev X* 2018;8:041035. DOI
42. Chi EO, Kim WS, Hur NH. Nearly zero temperature coefficient of resistivity in antiperovskite compound $CuNMn_3$. *Solid State Commun* 2001;120:307-10. DOI

43. Sun Y, Wang C, Chu L, Wen Y, Nie M, Liu F. Low temperature coefficient of resistivity induced by magnetic transition and lattice contraction in Mn_3NiN compound. *Scr Mater* 2010;62:686-9. DOI
44. Takenaka K, Ozawa A, Shibayama T, Kaneko N, Oe T, Urano C. Extremely low temperature coefficient of resistance in antiperovskite $Mn_3Ag_{1-x}Cu_xN$. *Appl Phys Lett* 2011;98:022103. DOI
45. Lin JC, Wang BS, Tong P, et al. Tunable temperature coefficient of resistivity in C- and Co-doped $CuNMn_3$. *Scr Mater* 2011;65:452-5. DOI
46. Deng S, Sun Y, Wang L, et al. Near-zero temperature coefficient of resistivity associated with magnetic ordering in antiperovskite $Mn_{3+x}Ni_{1-x}N$. *Appl Phys Lett* 2016;108:041908. DOI
47. He T, Huang Q, Ramirez AP, et al. Superconductivity in the non-oxide perovskite $MgCNi_3$. *Nature* 2001;411:54-6. DOI
48. Rosner H, Weht R, Johannes MD, Pickett WE, Tosatti E. Superconductivity near ferromagnetism in $MgCNi_3$. *Phys Rev Lett* 2002;88:027001. DOI PubMed
49. Wu M, Isshiki H, Chen T, Higo T, Nakatsuji S, Otani Y. Magneto-optical Kerr effect in a non-collinear antiferromagnet Mn_3Ge. *Appl Phys Lett* 2020;116:132408. DOI
50. Balk AL, Sung NH, Thomas SM, et al. Comparing the anomalous Hall effect and the magneto-optical Kerr effect through antiferromagnetic phase transitions in Mn_3Sn. *Appl Phys Lett* 2019;114:032401. DOI
51. Feng W, Guo GY, Zhou J, Yao Y, Niu Q. Large magneto-optical Kerr effect in noncollinear antiferromagnets Mn_3X (X = Rh, Ir, Pt). *Phys Rev B* 2015;92:144426. DOI
52. Kamishima K, Bartashevich M, Goto T, Kikuchi M, Kanomata T. Magnetic behavior of Mn_3GaC under high magnetic field and high pressure. *J Phys Soc Jpn* 1998;67:1748-54. DOI
53. Fruchart D, Bertaut EF, Sayetat F, Nasr Eddine M, Fruchart R, Sénateur JP. Structure magnetique de Mn_3GaC. *Solid State Commun* 1970;8:91-9. DOI
54. Fruchart D, Bertaut EF. Magnetic studies of the metallic perovskite-type compounds of manganese. *J Phys Soc Jpn* 1978;44:781-91. DOI
55. Çakır Ö, Acet M. Reversibility in the inverse magnetocaloric effect in Mn_3GaC studied by direct adiabatic temperature-change measurements. *Appl Phys Lett* 2012;100:202404. DOI
56. Sénateur JP, Boursier D, L'héritier P, Lorthioir G, Fruchart ME, Le Caer G. Etude par spectrometrie mössbauer de $ZnMn_3$ et de la transition antiferro-ferromagnetique de $GaMn_3C$ dopes au fer 57. *Mater Res Bull* 1974;9:603-14. DOI
57. Deng S, Sun Y, Wang L, et al. Frustrated triangular magnetic structures of Mn_3ZnN: applications in thermal expansion. *J Phys Chem C* 2015;119:24983-90. DOI
58. Fruchart D, Bertaut EF, Madar R, Fruchart R. Diffraction neutronique de Mn_3ZnN. *J Phys Colloques* 1971;32:C1-876. DOI
59. Wu M, Wang C, Sun Y, et al. Magnetic structure and lattice contraction in Mn_3NiN. *J Appl Phys* 2013;114:123902. DOI
60. Hua L, Wang L, Chen LF. First-principles investigation of Ge doping effects on the structural, electronic and magnetic properties in antiperovskite Mn_3CuN. *J Phys Condens Matter* 2010;22:206003. DOI
61. Han H, Sun Y, Deng S, et al. Effect of thermal stress on non-collinear antiferromagnetic phase transitions in antiperovskite Mn_3GaN compounds with Mn_3SbN inclusions. *Ceramics Int* 2022;48:15200-6. DOI
62. Sun Y, Hu P, Shi K, et al. Giant zero-field cooling exchange-bias-like behavior in antiperovskite $Mn_3Co_{0.61}Mn_{0.39}N$ compound. *Phys Rev Mater* 2019;3:024409. DOI
63. Salvador JR, Guo F, Hogan T, Kanatzidis MG. Zero thermal expansion in YbGaGe due to an electronic valence transition. *Nature* 2003;425:702-5. DOI
64. Mary TA, Evans JSO, Vogt T, Sleight AW. Negative Thermal Expansion from 0.3 to 1050 Kelvin in ZrW_2O_8. *Science* 1996;272:90-2. DOI
65. Song Y, Shi N, Deng S, Xing X, Chen J. Negative thermal expansion in magnetic materials. *Prog Mater Sci* 2021;121:100835. DOI
66. Chen J, Hu L, Deng J, Xing X. Negative thermal expansion in functional materials: controllable thermal expansion by chemical modifications. *Chem Soc Rev* 2015;44:3522-67. DOI PubMed
67. Gava V, Martinotto AL, Perottoni CA. First-principles mode Gruneisen parameters and negative thermal expansion in α-ZrW_2O_8. *Phys Rev Lett* 2012;109:195503. DOI PubMed
68. Li CW, Tang X, Muñoz JA, et al. Structural relationship between negative thermal expansion and quartic anharmonicity of cubic ScF_3. *Phys Rev Lett* 2011;107:195504. DOI
69. Long YW, Hayashi N, Saito T, Azuma M, Muranaka S, Shimakawa Y. Temperature-induced A-B intersite charge transfer in an A-site-ordered $LaCu_3Fe_4O_{12}$ perovskite. *Nature* 2009;458:60-3. DOI
70. Gerhardt I, Liu Q, Lamas-Linares A, Skaar J, Kurtsiefer C, Makarov V. Full-field implementation of a perfect eavesdropper on a quantum cryptography system. *Nat Commun* 2011;2:349. DOI PubMed
71. Chen J, Fan L, Ren Y, et al. Unusual transformation from strong negative to positive thermal expansion in $PbTiO_3$-$BiFeO_3$ perovskite. *Phys Rev Lett* 2013;110:115901. DOI
72. Huang R, Liu Y, Fan W, et al. Giant negative thermal expansion in $NaZn_{13}$-type La(Fe, Si, Co)$_{13}$ compounds. *J Am Chem Soc* 2013;135:11469-72. DOI
73. Qi TF, Korneta OB, Parkin S, De Long LE, Schlottmann P, Cao G. Negative volume thermal expansion via orbital and magnetic orders in $Ca_2Ru_{1-x}Cr_xO_4$ ($0 < x < 0.13$). *Phys Rev Lett* 2010;105:177203. DOI

74. Richter DD, Markewitz D, Trumbore SE, Wells CG. Rapid accumulation and turnover of soil carbon in a re-establishing forest. *Nature* 1999;400:56-8. DOI
75. Kiyama T, Yoshimura K, Kosuge K, Ikeda Y, Bando Y. Invar effect of $SrRuO_3$: itinerant electron magnetism of Ru 4*d* electrons. *Phys Rev B Condens Matter* 1996;54:R756-9. DOI PubMed
76. Taniguchi T, Mizusaki S, Okada N, et al. Anomalous volume expansion in $CaRu_{0.85}Fe_{0.15}O_3$: neutron powder diffraction and magnetic compton scattering. *Phys Rev B* 2007;75:024414. DOI
77. Klimczuk T, Walker HC, Springell R, et al. Negative thermal expansion and antiferromagnetism in the actinide oxypnictide NpFeAsO. *Phys Rev B* 2012:85. DOI
78. Uchishiba H. Antiferromagnetism of γ-phase manganese alloys containing Ni, Zn, Ga and Ge. *J Phys Soc Jpn* 1971;31:436-40. DOI
79. Yokoyama T, Eguchi K. Anisotropic thermal expansion and cooperative Invar and anti-Invar effects in mn alloys. *Phys Rev Lett* 2013;110:075901. DOI PubMed
80. Yu C, Lin K, Jiang S, et al. Plastic and low-cost axial zero thermal expansion alloy by a natural dual-phase composite. *Nat Commun* 2021;12:4701. DOI PubMed PMC